



Cite this: *CrystEngComm*, 2024, **26**, 2765

Large tensile-strained BaTiO_3 films grown on a lattice-mismatched La-doped BaSnO_3 bottom electrode[†]

Lizhikun Gong,^a Ko Marunouchi,^a Akira Chikamatsu,^{iD b} Hiromichi Ohta^{iD c} and Tsukasa Katayama^{iD *cd}

Perovskite BaTiO_3 has been widely studied and utilized in various applications owing to its high permittivity, ferroelectricity, and stability. However, its low ferroelectric-paraelectric phase transition temperature (T_C , 120 °C) limits its application. The T_C can be increased by applying an epitaxial strain provided by a lattice-mismatched substrate. However, applying large tensile strain on BaTiO_3 is difficult, especially when a bottom electrode is present. In this study, we successfully fabricated large tensile-strained BaTiO_3 films using La-doped BaSnO_3 bottom electrodes. A tensile strain of 2% was achieved, which is three times larger than that previously reported for BaTiO_3 films grown on bottom electrodes. By adjusting the thickness of the BaTiO_3 layer between 20 and 300 nm, tensile strain can be varied within the range of 0.6–2%. Remarkably, the T_C of the obtained films exceeds 400 °C. In addition, although it was considered that tensile-strained BaTiO_3 films have ferroelectric polarization in the in-plane direction, the 0.6% tensile-strained film showed ferroelectric polarization in the out-of-plane direction. This finding reveals that the ferroelectric polarization direction was slightly tilted away from the predominant in-plane direction of the film.

Received 1st March 2024,
Accepted 23rd April 2024

DOI: 10.1039/d4ce00197d

rsc.li/crystengcomm

1. Introduction

Perovskite BaTiO_3 is one of the most promising ferroelectric materials owing to its desirable properties such as high permittivity (ϵ_r), tunability of ϵ_r , piezoelectricity, and stability.^{1,2} It is widely used in electronic components such as multilayer ceramic capacitors and microwave devices.^{3–7} The properties of BaTiO_3 can be controlled by varying the strain from the substrate. For instance, in epitaxial BaTiO_3 film grown coherently on the DyScO_3 substrate, the remnant polarization value of the ferroelectric phase is significantly higher (70 $\mu\text{C cm}^{-2}$) compared to that of the bulk (24 $\mu\text{C cm}^{-2}$).⁸ Furthermore, BaTiO_3 films demonstrate a 500 °C increase in ferroelectric transition temperature (T_C) compared with the bulk (120 °C).⁸ In addition, a flexoelectric effect occurs, causing the alignment of the polarization direction in

the out-of-plane direction without the application of an electric field.^{8–10}

The magnitude of substrate-induced strain can be controlled by selecting the substrates, bottom electrodes, and film thickness. For instance, when BaTiO_3 films were coherently grown on SrTiO_3 ($a = 3.905 \text{ \AA}$) or GdScO_3 ($a = 3.965 \text{ \AA}$) substrates, compressive strains of 2 and 0.7% were induced in the films, respectively,^{8,11} whereas bulk BaTiO_3 exhibited a tetragonal perovskite structure with $a = 3.992$ and $c = 4.036 \text{ \AA}$. Such application of compressive strain increases in remnant polarization (P_r), which is associated with an increase in the c/a ratio.^{8–12} Conversely, the application of tensile strain on BaTiO_3 films has also been investigated using substrates with large lattice constants such as MgO ($a = 4.213 \text{ \AA}$) and MgAl_2O_4 ($a/2 = 4.042 \text{ \AA}$).^{13–18} The films showed an enhancement in T_C (200–220 °C) and ferroelectricity along the in-plane direction.^{17,18} However, these substrates are insulators, and it is difficult to prepare bottom electrodes while maintaining a high tensile strain on the BaTiO_3 layer. In fact, in previously prepared BaTiO_3 films with bottom electrodes, tensile strain was limited to 0.57%.^{19,20} To achieve a large tensile strain in the BaTiO_3 film, we investigated La-doped BaSnO_3 (LBSO, hereafter) epitaxial films as electrodes because they have a cubic perovskite structure with $a = 4.116 \text{ \AA}$, which is 3% longer compared to BaTiO_3 and exhibits rather high electrical conductivity over 10^3 S cm^{-1} at room

^a Graduate School of Information Science and Technology, Hokkaido University, N14W9, Sapporo 060-0814, Japan

^b Department of Chemistry, Faculty of Science, Ochanomizu University, 2-1-1 Otsuka, Bunkyo, Tokyo 112-8610, Japan

^c Research Institute for Electronic Science, Hokkaido University, N20W10, Sapporo 001-0020, Japan. E-mail: katayama@es.hokudai.ac.jp

^d JST-PRESTO, Kawaguchi, Saitama 332-0012, Japan

[†] Electronic supplementary information (ESI) available: See ESI for the details of AFM images of the BaTiO_3 films. See DOI: <https://doi.org/10.1039/d4ce00197d>



temperature.^{21–27} In this study, we investigated the crystal structures and ferroelectric properties of tensile-strained BaTiO_3 films grown on 50 nm-thick LBSO bottom electrodes prepared on SrTiO_3 (001) (STO) substrates. By adjusting the film thickness, the tensile strain values can be varied between 0.6 and 2%. The T_C of the 0.6 and 1.3%-tensile-strained films were ~ 400 and ~ 500 °C, respectively, which is significantly higher than that of the bulk BaTiO_3 (120 °C). In case of the polarization *versus* electric field (P - E) curves, ferroelectric behavior did not appear along the out-of-plane direction for the 1.4–2%-tensile strained films probably because the ferroelectric polarization appears in the in-plane direction. On the contrary, the 0.6%-tensile-strained film also exhibited ferroelectric polarization along the out-of-plane direction, suggesting that the ferroelectric polarization direction was slightly tilted away from the in-plane direction.

2. Experimental

Epitaxial films of BaTiO_3 were fabricated on LBSO (2% La-doped, $\text{La}_{0.02}\text{Ba}_{0.98}\text{SnO}_3$)-buffered SrTiO_3 (001) substrates using a pulsed laser deposition (PLD) technique.²⁴ During the deposition, the substrate temperature, laser energy, and oxygen partial pressure were maintained at 850 °C, 0.5 J cm^{-2} pulse⁻¹, and 0.5 Pa for the BaTiO_3 layer and 750 °C, 2 J cm^{-2} pulse⁻¹, and 20 Pa for the LBSO layer, respectively. The typical thickness of the LBSO layer is 50 nm.

The crystal structures of the obtained films were evaluated using high-resolution X-ray diffraction (XRD, ATX-G, Rigaku Co.) with $\text{Cu K}\alpha_1$ radiation and variable-temperature XRD (D8 Discover, Bruker AXS GmbH) with $\text{Cu K}\alpha_1$ and $\text{K}\alpha_2$ radiation. The film thicknesses were determined by analyzing the Pendellösung fringes around the Bragg diffraction peaks and X-ray reflectivity. For the calculation of strain, we employed the formula: strain = $a_{\text{film}}/a_{\text{bulk}} - 1$, which is commonly used in previous literature. The surface morphology was observed by atomic force microscopy (AFM, Nanocute, Hitachi High-tech). The ferroelectric properties of the films were measured using a ferroelectric tester (Multiferroic II, Radian Inc.). In the measurement, an 80 nm-thick Pt electrode with a diameter of 100 μm was used as the top electrode, whereas the LBSO layer was used as the bottom electrode.

3. Results and discussion

Fig. 1 shows the out-of-plane XRD patterns of the BaTiO_3 films as functions of the BaTiO_3 thickness (t_{BTO}). The films were grown on the LBSO bottom electrodes prepared on STO substrates. The range of t_{BTO} is set to 20–300 nm. The (002) diffraction peaks of LBSO and BaTiO_3 appear at $q_z/2\pi = 4.85$ and 5.00–5.02 nm^{-1} , respectively. In addition, clear Pendellösung fringes were observed around the (002) diffraction peaks of LBSO, indicating the highly (001) orientation of the LBSO bottom electrode layer. On the contrary, the (002) diffraction peaks of BaTiO_3 shift toward a

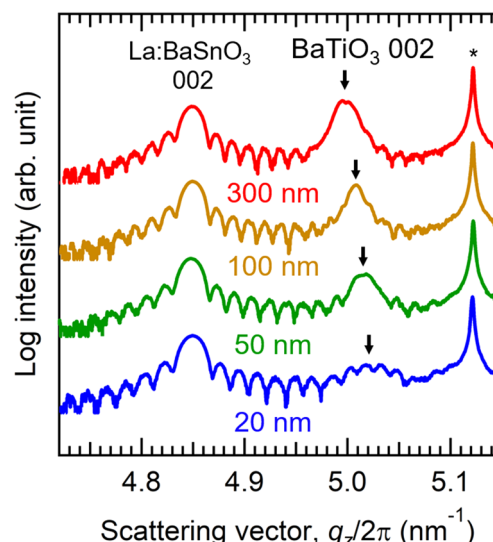


Fig. 1 Out-of-plane XRD patterns of the BaTiO_3 films with varied thickness grown on LBSO/STO substrates. The asterisk indicates the (002) STO substrate peak.

lower $q_z/2\pi$ side with increasing t_{BTO} . As the t_{BTO} increases from 20 to 300 nm, the *c*-axis length of the BaTiO_3 layer increases from 3.979 to 4.006 \AA . The *c*-axis lengths were shorter than those of bulk BaTiO_3 ($c = 4.036 \text{\AA}$), indicating the presence of tensile strain within the films. Fig. S1† shows the film surface morphologies. The root mean square roughness values are smaller than 0.3 nm, confirming the atomically flat surface of the films.

Fig. 2 shows the reciprocal space mappings (RSMs) around the (103) diffraction spot for the BaTiO_3 film with varied thicknesses. In case of the LBSO layer, the in-plane *a*-axis length (4.08 \AA) is shorter than the out-of-plane *c*-axis length (4.125 \AA) owing to the compressive strain from the STO

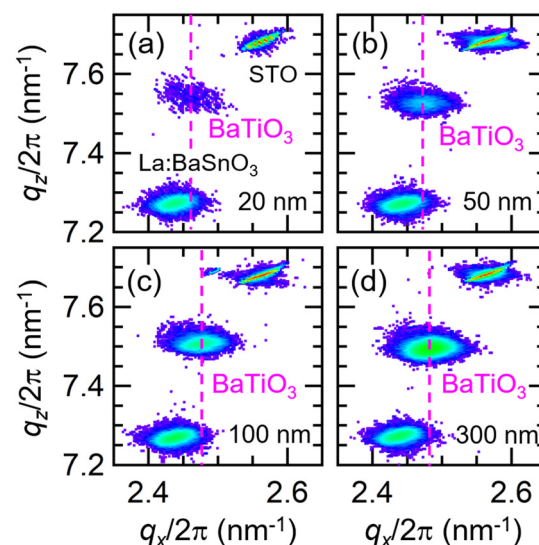


Fig. 2 Reciprocal space mappings for the BaTiO_3 film around the (103) diffraction spots. $t_{\text{BTO}} =$ (a) 20, (b) 50, (c) 100, and (d) 300 nm.



substrate. The (103) diffraction spot of BaTiO_3 was observed as a single spot without splitting, indicating that the BaTiO_3 layer had a tetragonal structure. With increasing t_{BTO} , the diffraction spot of BaTiO_3 shifts toward the higher $q_z/2\pi$ side. The a -axis lengths of the BaTiO_3 films are in the range of 4.01–4.07 Å, which is shorter than that of the LBSO layer, whereas it is longer than that of bulk BaTiO_3 . These results confirmed the presence of tensile strain in the BaTiO_3 films.

Fig. 3(a) shows the lattice constants of the BaTiO_3 films as a function of t_{BTO} . Remarkably, the c -axis was shorter than the a -axis length, in contrast to the behavior observed for bulk BaTiO_3 . With increasing t_{BTO} , the a (c) values of the films monotonically increased (decreased) and approached those of the bulk single crystal. Fig. 3(b) shows the tensile strain values of the BaTiO_3 films. At $t_{\text{BTO}} = 20$ nm, the tensile strain value is as high as 2.0%, which is much higher than the previous report on epitaxially grown BaTiO_3 films on MgO substrate with the bottom electrode layer (<0.57%).^{19,20} The tensile strain value decreases with increasing t_{BTO} and reaches 0.6% at $t_{\text{BTO}} = 300$ nm. The decrease in the tensile strain with increasing t_{BTO} was attributed to the relaxation of the in-plane lattice with increasing distance from the substrate because of the generation of dislocations in the film.^{28,29}

The BaTiO_3 films were deposited using PLD at a substrate temperature (T_s) of 850 °C and an oxygen partial pressure (P_{O_2}) of 0.5 Pa, with a laser energy of 0.5 J cm^{-2} pulse⁻¹. Notably, PLD conditions are known to influence the lattice strain and properties of BaTiO_3 films. For instance, the c/a values decrease with increasing T_s for BaTiO_3 films grown on multilayer-buffered Si substrates.³⁰ Additionally, it has been reported that oxygen vacancies are introduced at low P_{O_2} ,

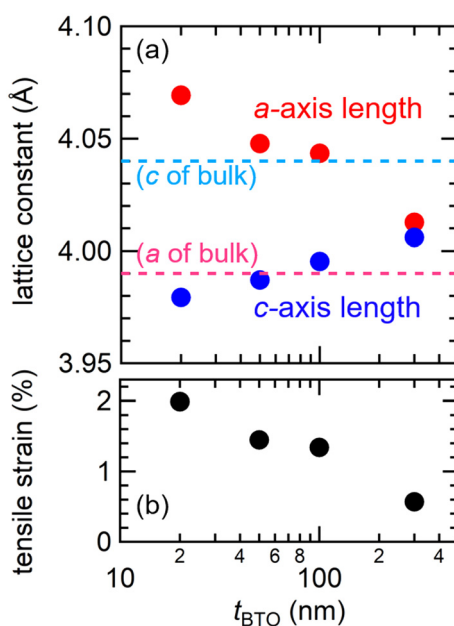


Fig. 3 (a) Lattice constants and (b) tensile strain values for the BaTiO_3 films as a function of t_{BTO} . Figure (a) also includes the a - and c -axis lengths of bulk BaTiO_3 .⁸

while high P_{O_2} results in locally incoherent grain boundaries in BaTiO_3 films.³¹ Moreover, high laser energy has been shown to increase the growth-induced defect structures and create defect dipoles in BaTiO_3 films.⁹ Hence, in this study, the influence of lattice strain due to defects induced by PLD conditions may affect the properties alongside the effects of strain provided by the substrate.

Fig. 4(a) illustrates the temperature (T) dependence of the out-of-plane XRD patterns of the BaTiO_3 film with t_{BTO} of 300 nm. To facilitate an understanding of the temperature-dependent changes in the BaTiO_3 peak position, the horizontal axis is normalized by the SrTiO_3 peak position, where $2\theta_{\text{STO}}$ and $2\theta_{\text{BTO}}$ represent the 2θ values of the SrTiO_3 (002) and BaTiO_3 (002) diffraction peaks, respectively. The XRD equipment used for temperature dependence differs from that used at room temperature (refer to Fig. 1–3, see experimental section). For $t_{\text{BTO}} = 100$ and 300 nm, the curves of $2\theta_{\text{BTO}} - 2\theta_{\text{STO}}$ versus T exhibit kinks at ~500 and ~400 °C, respectively (Fig. 4(b)). Since bulk SrTiO_3 is known not to undergo phase transitions in its crystal structure, the observed kinks are attributed to changes in the lattice constants of the BaTiO_3 films. Such a change in lattice

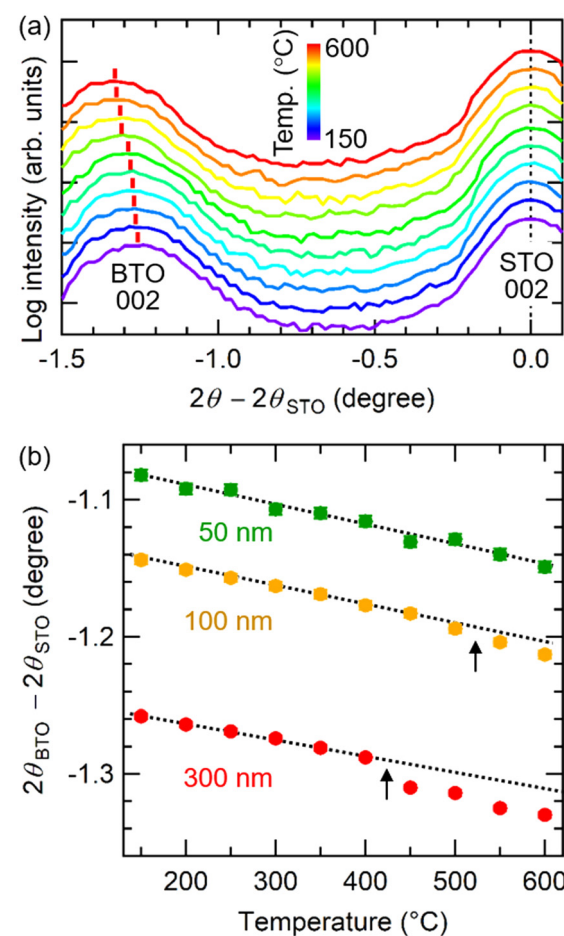


Fig. 4 (a) Temperature dependence of the out-of-plane XRD patterns for the BaTiO_3 film with $t_{\text{BTO}} = 300$ nm. (b) The $2\theta_{\text{BTO}} - 2\theta_{\text{STO}}$ values as a function of T for the BaTiO_3 films with varied thickness.

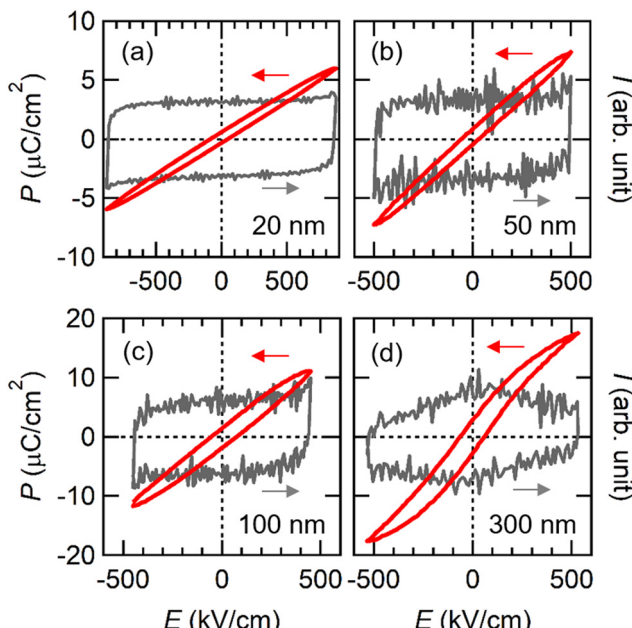


Fig. 5 P - E and I - E curves of the BaTiO_3 films with thickness of (a) 20, (b) 50, (c) 100, and (d) 300 nm.

constants has also been observed in bulk and film BaTiO_3 owing to a transition from the ferroelectric tetragonal phase ($P4mm$) to the paraelectric cubic phase ($Pm3m$).⁸ Thus, the observed kinks in the films with $t_{\text{BTO}} = 100$ and 300 nm were derived from ferroelectric-to-paraelectric phase transitions. Choi *et al.* predicted the T_C values of BaTiO_3 film under biaxial in-plane strain based on thermodynamic analysis;⁸ the predicted T_C was in the ranges of 300–500 °C and 400–800 °C when 0.6 and 1.3%-tensile strains were applied to the BaTiO_3 film, respectively. These predicted T_C values are consistent with our results: T_C for the $t_{\text{BTO}} = 100$ and 300 nm films with a tensile strain of 0.6 and 1.3% were ~400 and ~500 °C, respectively. On the other hand, no obvious kinks were observed in the $2\theta_{\text{BTO}} - 2\theta_{\text{STO}}$ values *versus* T curves for the BaTiO_3 films with $t_{\text{BTO}} = 20$ and 50 nm below 600 °C.

Fig. 5 shows the polarization *versus* electric field (P - E) curve for BaTiO_3 films with $t_{\text{BTO}} = 20, 50, 100$, and 300 nm. The measurements were conducted at 25 °C and a frequency of 10 kHz. At $t_{\text{BTO}} = 20$ nm and 50 nm, no ferroelectric hysteresis loops were observed in the out-of-plane direction. This is probably because the ferroelectric polarization was completely along the in-plane direction, as observed in a previously reported BaTiO_3 film under tensile strain.^{12,17} It is noted that bulk BaTiO_3 with a perovskite structure exhibits tetragonal, orthorhombic, and rhombohedral symmetries below the ferroelectric transition temperature. While the polarization of the tetragonal phase aligns along the c -axis, that of the orthorhombic and rhombohedral phases align along the [110] and [111] directions, respectively.³² The direction of polarization is primarily determined by the availability of spatial regions where Ti ions can undergo displacement. For instance, in tetragonal BaTiO_3 with $c > a$,

there is spatial freedom for Ti ions along the c -axis direction, leading to spontaneous polarization along the c -axis. In our case, the BaTiO_3 film exhibits a tetragonal structure ($a = b \neq c$) with the a -axis length longer than the c -axis length. Consequently, the location of the spatial region available for Ti ion displacement differs from that of the bulk material, resulting in a change in the polarization direction.

In contrast, at $t_{\text{BTO}} = 300$ nm, a ferroelectric hysteresis loop was observed, accompanied by polarization-switching current peaks. The P_r value in the out-of-plane direction was 3 $\mu\text{C cm}^{-2}$. This suggests that the ferroelectric polarization direction was slightly tilted away from the in-plane direction at $t_{\text{BTO}} = 300$ nm because of the weaker tensile strain (0.6%) compared to other films (1.3–2%).

4. Conclusions

To achieve high tensile strain on the BaTiO_3 film with the bottom electrode, we fabricated BaTiO_3 films on a LBSO bottom electrode. The tensile strain values increase from 0.6 to 2% with decreasing thickness from 300 to 20 nm. The T_C values of the 0.6 and 1.3%-tensile strained films are ~400 and ~500 °C, respectively, which are much higher than those of the bulk (120 °C) and previously reported tensile-strained films (220–220 °C). For the 1.4–2% tensile-strained sheet, the ferroelectric hysteresis loops were not observed in the out-of-plane direction, probably because the ferroelectric polarization aligns in the in-plane direction owing to the tensile strain. On the contrary, the 0.6%-tensile strained film displayed ferroelectric behavior along the out-of-plane direction, suggesting that the ferroelectric polarization direction was slightly tilted away from the in-plane direction.

Conflicts of interest

The authors declare no competing financial interest.

Acknowledgements

This work was supported by JST, PRESTO Grant Number JPMJPR21Q3, Japan, JSPS KAKENHI (20H02614 (TK)), and the Kao Foundation for Arts and Sciences (T.K.). H.O. was supported by a Grant-in-Aid for Scientific Research on Innovative Areas (19H05791) from JSPS. L.G. was supported by China Scholarships Council 202008050264.

References

- 1 F. A. Ismail, R. A. M. Osman and M. S. Idris, Review on dielectric properties of rare earth doped barium titanate, *AIP Conf. Proc.*, 2016, 1756.
- 2 G. H. Haertling, Ferroelectric ceramics: history and technology, *J. Am. Ceram. Soc.*, 1999, **82**, 797–818.
- 3 S.-H. Yoon, M.-Y. Kim, C.-H. Nam, J.-W. Seo, S.-K. Wi and K.-H. Hur, Grain-growth effect on dielectric nonlinearity of BaTiO_3 -based multi-layer ceramic capacitors, *Appl. Phys. Lett.*, 2015, **107**, 072906.



4 A. Feteira, D. C. Sinclair, I. M. Reaney, Y. Somiya and M. T. Lanagan, BaTiO₃-based ceramics for tunable microwave applications, *J. Am. Ceram. Soc.*, 2004, **87**, 1082–1087.

5 Y.-F. Zhu, L. Zhang, T. Natsuki, Y.-Q. Fu and Q.-Q. Ni, Facile synthesis of BaTiO₃ nanotubes and their microwave absorption properties, *ACS Appl. Mater. Interfaces*, 2012, **4**(4), 2101–2106.

6 M. Acosta, N. Novak, V. Rojas, S. Patel, R. Vaish, J. Koruza, G. A. Rossetti and J. Rödel, BaTiO₃-based piezoelectrics: Fundamentals, current status, and perspectives, *Appl. Phys. Rev.*, 2017, **4**(4), 041305.

7 M. P. McNeal, S.-J. Jang and R. E. Newnham, The effect of grain and particle size on the microwave properties of barium titanate (BaTiO₃), *J. Appl. Phys.*, 1998, **83**, 3288–3297.

8 K. J. Choi, M. Biegalski, Y. Li, A. Sharan, J. Schubert, R. Uecker, P. Reiche, Y. Chen, X. Pan and V. Gopalan, Enhancement of ferroelectricity in strained BaTiO₃ thin films, *Science*, 2004, **306**, 1005–1009.

9 A. R. Damodaran, E. Breckenfeld, Z. Chen, S. Lee and L. W. Martin, Enhancement of Ferroelectric Curie Temperature in BaTiO₃ Films via Strain-Induced Defect Dipole Alignment, *Adv. Mater.*, 2014, **26**, 6341–6347.

10 R. Guo, L. Shen, H. Wang, Z. Lim, W. Lu, P. Yang, Ariando, A. Gruverman, T. Venkatesan, Y. P. Feng and J. Chen, Tailoring Self-Polarization of BaTiO₃ Thin Films by Interface Engineering and Flexoelectric Effect, *Adv. Mater. Interfaces*, 2016, **3**, 1600737.

11 O. Trithaveesak, J. Schubert and C. Buchal, Ferroelectric properties of epitaxial BaTiO₃ thin films and heterostructures on different substrates, *J. Appl. Phys.*, 2005, **98**, 114101.

12 D. G. Schlom, L.-Q. Chen, C.-B. Eom, K. M. Rabe, S. K. Streiffer and J.-M. Triscone, Strain tuning of ferroelectric thin films, *Annu. Rev. Mater. Res.*, 2007, **37**, 589–626.

13 L. Beckers, J. Schubert, W. Zander, J. Ziesmann, A. Eckau, P. Leinenbach and C. Buchal, Structural and optical characterization of epitaxial waveguiding BaTiO₃ thin films on MgO, *J. Appl. Phys.*, 1998, **83**, 3305–3310.

14 I. Misirlioglu, S. Alpay, F. He and B. Wells, Stress induced monoclinic phase in epitaxial BaTiO₃ on MgO, *J. Appl. Phys.*, 2006, **99**, 104103.

15 C. Buchal, L. Beckers, A. Eckau, J. Schubert and W. Zander, Epitaxial BaTiO₃ thin films on MgO, *Mater. Sci. Eng.*, **B**, 1998, **56**, 234–238.

16 C. Lei, The growth of BaTiO₃ films on (001) MgAl₂O₄ substrates by pulsed laser deposition technique, *Thin Solid Films*, 2006, **515**, 1701–1707.

17 K. Komatsu, I. Suzuki, T. Aoki, Y. Hamasaki, S. Yasui, M. Itoh and T. Taniyama, In-plane ferroelectricity and enhanced Curie temperature in perovskite BaTiO₃ epitaxial thin films, *Appl. Phys. Lett.*, 2020, **117**, 072902.

18 S. Kumar, D. Kumar, V. Sathe, R. Kumar and T. Sharma, Absence of low temperature phase transitions and enhancement of ferroelectric transition temperature in highly strained BaTiO₃ epitaxial films grown on MgO Substrates, *J. Appl. Phys.*, 2015, **117**, 134103.

19 F. He and B. O. Wells, Lattice strain in epitaxial BaTiO₃ thin films, *Appl. Phys. Lett.*, 2006, **88**, 152908.

20 W. Zhang, L. Kang, M. Yuan, Q. Yang and J. Ouyang, Effect of bottom electrode on the microstructure and electrical properties of sputtered BaTiO₃ films on MgO substrates, *J. Alloys Compd.*, 2013, **580**, 363–368.

21 Q. Liu, J. Dai, Y. Zhang, H. Li, B. Li, Z. Liu and W. Wang, High electrical conductivity in oxygen deficient BaSnO₃ films, *J. Alloys Compd.*, 2016, **655**, 389–394.

22 H. J. Cho, B. Feng, T. Onozato, M. Wei, A. V. Sanchela, Y. Ikuhara and H. Ohta, Investigation of electrical and thermal transport property reductions in La-doped BaSnO₃ films, *Phys. Rev. Mater.*, 2019, **3**, 094601.

23 A. Prakash, P. Xu, A. Faghaninia, S. Shukla, J. W. Ager III, C. S. Lo and B. Jalan, Wide bandgap BaSnO₃ films with room temperature conductivity exceeding 10⁴ S cm⁻¹, *Nat. Commun.*, 2017, **8**, 15167.

24 A. V. Sanchela, M. Wei, H. Zensyo, B. Feng, J. Lee, G. Kim, H. Jeen, Y. Ikuhara and H. Ohta, Large thickness dependence of the carrier mobility in a transparent oxide semiconductor, La-doped BaSnO₃, *Appl. Phys. Lett.*, 2018, **112**, 232102.

25 H. J. Cho, T. Onozato, M. Wei, A. Sanchela and H. Ohta, Effects of vacuum annealing on the electron mobility of epitaxial La-doped BaSnO₃ films, *APL Mater.*, 2019, **7**, 022507.

26 A. V. Sanchela, M. Wei, J. Lee, G. Kim, H. Jeen, B. Feng, Y. Ikuhara, H. J. Cho and H. Ohta, Buffer layer-less fabrication of a high-mobility transparent oxide semiconductor, La-doped BaSnO₃, *J. Mater. Chem. C*, 2019, **7**, 5797–5802.

27 L. Gong, R. Yu, H. Ohta and T. Katayama, Synthesis and transparent conductivity of crack-free La: BaSnO₃ epitaxial flexible sheets, *Dalton Trans.*, 2023, **52**, 6317–6323.

28 H. Sun, W. Tian, X. Pan, J. H. Haeni and D. G. Schlom, Evolution of dislocation arrays in epitaxial BaTiO₃ thin films grown on (100) SrTiO₃, *Appl. Phys. Lett.*, 2004, **84**, 3298–3300.

29 T. Suzuki, Y. Nishi and M. Fujimoto, Analysis of misfit relaxation in heteroepitaxial BaTiO₃ thin films, *Philos. Mag. A*, 1999, **79**, 2461–2483.

30 J. Lyu, I. Fina, R. Solanas, J. Fontcuberta and F. Sanchez, Tailoring Lattice Strain and Ferroelectric Polarization of Epitaxial BaTiO₃ Thin Films on Si(001), *Sci. Rep.*, 2018, **8**, 495.

31 J. Lyu, S. Estandia, J. Gazquez, F. M. Chisholm, I. Fina, N. Dix, J. Fontcuberta and F. Sanchez, Control of Polar Orientation and Lattice Strain in Epitaxial BaTiO₃ Films on Silicon, *ACS Appl. Mater. Interfaces*, 2018, **10**, 25529–25535.

32 J. Fujioka, A. Doi, D. Okuyama, D. Morikawa, T. Arima, K. N. Okada, Y. Kaneko, T. Fukuda, H. Uchiyama, D. Ishikawa, A. Q. R. Baron, K. Kato, M. Takata and Y. Tokura, Ferroelectric-like metallic state in electron doped BaTiO₃, *Sci. Rep.*, 2015, **5**, 13207.

